Chinese Journal of Oceanology and Limnology
Vol. 26 No. 4, P. 450-458, 2008
DOI: 10.1007/s00343-008-0450-4

Propagation of internal waves up continental slope and shelf *

DAI Dejun (戴德君) [†,††,**], WANG Wei (王伟) [†††], QIAO Fangli (乔方利) [†,††],
YUAN Yeli (袁业立) [†,††], XIANG Wenxi (相文玺) [††††]
[†] *The First Institute of Oceanography, SOA, Qingdao 266061, China*
[††] *Key Laboratory of Marine Science and Numerical Modeling, SOA, Qingdao 266061, China*
[†††] *Physical Oceanography Laboratory, Ocean University of China, Qingdao 266003, China*
[††††] *National Marine Data and Information Service, Tianjin 300171, China*

Received June 23, 2006; revision accepted Mar. 30, 2007

Abstract In a two-dimensional and linear framework, a transformation was developed to derive eigensolutions of internal waves over a subcritical hyperbolic slope and to approximate the continental slope and shelf. The transformation converts a hyperbolic slope in physical space into a flat bottom in transform space while the governing equations of internal waves remain hyperbolic. The eigensolutions are further used to study the evolution of linear internal waves as it propagates to subcritical continental slope and shelf. The stream function, velocity, and vertical shear of velocity induced by internal wave at the hyperbolic slope are analytically expressed by superposition of the obtained eigensolutions. The velocity and velocity shear increase as the internal wave propagates to a hyperbolic slope. They become very large especially when the slope of internal wave rays approaches the topographic slope, which is consistent with the previous studies.

Keyword: internal waves; velocity and velocity shear; hyperbolic slope; transform method

1 INTRODUCTION

Internal waves are those that take place in a stratified fluid. The largest vertical displacement of internal waves occurs within the fluid and opposed to that of the surface waves. Due to its importance on the diapycnal mixing, generation and propagation of internal waves over oceanic topography become an active topic of physical oceanography (Wunsch and Ferrari, 2004; Dai et al., 2005; Nash et al., 2006; Petrelis et al., 2006). It is well known that the linear internal waves may evolve into nonlinear solitary waves when they propagate to a continental slope, as shown by many previous studies (Liu et al., 1998; Cai and Gan, 2001; Fang and Du, 2005). Additional to the nonlinear evolution, there are still many linear and important processes which need further investigation, such as reflection and scattering of internal waves when internal waves propagate to the continental slope (Baines, 1971a, b; Müller and Liu, 2000a, b). In this paper, scattering of internal waves means the redistribution of incoming energy flux in physical space and mode number range when the linear internal waves propagate to sloping topography (Müller and Liu, 2000a, b). The reflection and scattering processes have been studied by previous researches since the redistribution of energy flux is helpful for studying the diapycnal mixing (Phillips, 1977; Müller and Liu, 2000a, b).

Reflection of internal waves off an infinite linear slope was studied in two-dimensional framework by Phillips (1977) while Wunsch (1968) provided an eigensolutions of internal waves propagating to a subcritical linear slope. A linear slope can give a good approximation for several actual topographies while the curved topography is common in the

* Supported by the National Nature Science Foundation of China (No. 40406008 and 40876015) and the Foundation for Open Projects of the Key Lab of Physical Oceanography, The Ministry of Education, China (No. 200309).
** Corresponding author: djdai@fio.org.cn

ocean. Baines (1971a, b) employed a ray-tracing method and reduced the reflection of internal waves off a curved slope to solve coupled Fredholm integral equations of the second type. Müller and Liu (2000a, b) used a mapping function based on ray tracing to study scattering of internal waves at finite topography in two dimensions. Unfortunately, the ray-tracing method is complicated and it is inconvenient to use numerical results for further theoretical analysis. Therefore, finding eigen-solutions of internal waves over a curved slope is still an important topic for studying the reflection or scattering process.

In this study, a transformation was developed to derive eigensolutions of internal waves at a subcritical hyperbolic slope. The hyperbolic slope can approximate vertical sections of many bottom topographies, such as continental slope and shelf. The eigensolutions are used to discuss the evolution of internal waves in linear framework as they propagate from deep ocean to hyperbolic slope.

2 EIGENSOLUTIONS OF INTERNAL WAVES AT HYPERBOLIC SLOPE

For a continental slope, a dextral Cartesian coordinate system is set up as follows: $\tilde{x}$ represents a cross-slope axis positive shoreward; $\tilde{y}$ represents an axis along continental slope, and $\tilde{z}$, a vertical axis positive up. In most of the real oceans, the length of continental slope, i.e., the scale along the continental slope, is generally much larger than the width. It implies that the gradients of variables along $\tilde{y}$ axis can be ignored compared with those along $\tilde{x}$ axis. Then a two-dimensional framework is used to describe the internal waves. In a two-dimensional framework, dimensional internal wave equation is given (Appendix A):

$$\frac{\partial^4\tilde{\varphi}}{\partial\tilde{x}^2\partial\tilde{t}^2}+\frac{\partial^4\tilde{\varphi}}{\partial\tilde{z}^2\partial\tilde{t}^2}+\tilde{f}^2\frac{\partial^2\tilde{\varphi}}{\partial\tilde{z}^2}+\tilde{N}^2\frac{\partial^2\tilde{\varphi}}{\partial\tilde{x}^2}=0 \qquad (1)$$

where $\tilde{N}$ is the Brunt-Väisälä frequency; $\tilde{f}$ the Coriolis parameter; $\tilde{\varphi}$ the stream function which lets $\tilde{u}=-\partial\tilde{\varphi}/\partial\tilde{z}, \tilde{w}=\partial\tilde{\varphi}/\partial\tilde{x}$; and $(\tilde{u},\tilde{w})$ are the dimensional velocity components corresponding to $(\tilde{x},\tilde{z})$. The boundary conditions are:

$$\tilde{\varphi}=0, \qquad \text{at} \quad \tilde{z}=0, \tilde{z}=\tilde{h}(\tilde{x}) \qquad (2)$$

where $\tilde{z}=\tilde{h}(\tilde{x})$ is the bottom boundary. Eq.1 describes the internal wave whose frequency $\tilde{\omega}$ is much greater than the Coriolis parameter, i.e., $\tilde{\omega}\gg\tilde{f}$.

Generally, the non-dimensional equations are more convenient. Introduce:

$$\tilde{\varphi}=\tilde{\psi}\varphi, \quad \tilde{x}=\tilde{H}x, \quad \tilde{z}=\tilde{H}z, \\ \tilde{t}=\frac{1}{\tilde{f}}t, \quad \tilde{N}=\tilde{f}N \qquad (3)$$

where $\tilde{\psi}$ is the amplitude of $\tilde{\varphi}$; $\tilde{H}$, the maximum water depth of the studies area. We then can obtain:

$$\frac{\tilde{\psi}\tilde{f}^2}{\tilde{H}^2}\left[\frac{\partial^4\varphi}{\partial x^2\partial t^2}+\frac{\partial^4\varphi}{\partial z^2\partial t^2}+\frac{\partial^2\varphi}{\partial z^2}+N^2\frac{\partial^2\varphi}{\partial x^2}\right]=0. \qquad (4)$$

This equation can be reduced to:

$$\frac{\partial^4\varphi}{\partial x^2\partial t^2}+\frac{\partial^4\varphi}{\partial z^2\partial t^2}+\frac{\partial^2\varphi}{\partial z^2}+N^2\frac{\partial^2\varphi}{\partial x^2}=0 \qquad (5)$$

which is also the non-dimensional equation. In the following part, the non-dimensional equation is applied to discuss the propagation of internal wave to a curved slope. For a monochromatic wave with frequency ω, let $\varphi=\phi(x,z)\exp(\mathrm{i}\omega t)$, then

$$\phi_{zz}-\frac{1}{c^2}\phi_{xx}=0 \qquad (6)$$

where

$$c^2=\frac{\omega^2-1}{N^2-\omega^2} \qquad (7)$$

The boundary conditions become

$$\phi=0, \qquad \text{at} \quad z=0, z=h(x) \qquad (8)$$

Assuming $N=const$, then $c=const$.

If the bottom is flat, i.e., $h(x)=-1$, it is easy to get the eigensolutions of Eq.6,

$$\phi_n=\sin(k_n z)\left[A_n\cos(k_n x)+B_n\sin(k_n x)\right] \qquad (9)$$

where $k_n=n\pi$, $n=1,2,3...$. However, the flat bottom is only a special case, the actual bottom topography is usually complex and irregular. Generally speaking, it is difficult to find the eigensolutions of Eq.6 when *h(x)* changes with *x*, which is the reason why ray-tracing method is used to study the propagation of internal waves to a curved topography.

Wunsch (1968) obtained the eigensolutions of internal waves at a subcritical linear slope $h(x)=rx$ in the polar coordinates, the solutions in Cartesian coordinates are:

$$\begin{aligned}\varphi_n &= A_n\left\{\sin[q_n\ln(cx-z)]-\sin[q_n\ln(cx+z)]\right\}\\ &\quad \exp(\mathrm{i}\omega t)\\ \varphi_n &= A_n\left\{\cos[q_n\ln(cx-z)]-\cos[q_n\ln(cx+z)]\right\}\\ &\quad \exp(\mathrm{i}\omega t)\end{aligned} \tag{10}$$

where $q_n=\dfrac{2n\pi}{\ln(c-r/c+r)}$, $n=1,2,3...$

It is obvious that the governing equation and the boundary conditions are all satisfied. Wunsch's solutions revealed that it is possible to get the eigensolutions of internal waves at a subcritical curved slope if a proper method is used. In the following text, a transformation is introduced to derive the eigensolutions of internal waves at a subcritical hyperbolic slope.

Introduce the following transformation

$$\begin{cases}\xi=(cx-z)^2-(cx+z)^2\\ \eta=(cx-z)^2+(cx+z)^2\end{cases} \tag{11}$$

into the governing Eq.6, yield (see Appendix B):

$$\begin{aligned}&\frac{\partial^2\phi}{\partial\xi^2}[16(cx-z)(cx+z)]+\\ &\frac{\partial^2\phi}{\partial\eta^2}[-16(cx-z)(cx+z)]=0\end{aligned} \tag{12}$$

The transformation converts the upper boundary $z=0$ to $\xi=0$ and the hyperbolic slope

$$h(x)=\frac{r}{x} \text{ to } \xi_0=-4cr\,.$$

Moreover, $16(cx-z)(cx+z)\neq 0$ for subcritical topography, then Eq.6 can be simplified to

$$\frac{\partial^2\phi}{\partial\xi^2}-\frac{\partial^2\phi}{\partial\eta^2}=0 \tag{13}$$

Therefore, the eigensolutions of internal waves at a subcritical hyperbolic slope is obtained

$$\begin{aligned}\phi_n &= A_n\sin(q_n\xi)\sin(q_n\eta)\\ \phi_n &= A_n\sin(q_n\xi)\cos(q_n\eta)\end{aligned} \tag{14}$$

where $q_n=n\pi/\xi_0$, $n=1,2,3....$ The eigensolutions in Cartesian coordinates are

$$\begin{aligned}\varphi_n &= \frac{A_n}{2}[\sin 2q_n(cx-z)^2-\sin 2q_n(cx+z)^2]\\ &\quad \exp(\mathrm{i}\omega t)\\ \varphi_n &= -\frac{A_n}{2}[\cos 2q_n(cx-z)^2-\cos 2q_n(cx+z)^2]\\ &\quad \exp(\mathrm{i}\omega t)\end{aligned} \tag{15}$$

It is obvious that Eq.15 is exactly the solutions of Eq.5 with a hyperbolic bottom boundary $h(x)=r/x$. Compared with the linear slope that studied by Wunsch (1968), the slope of hyperbolic topography changes along *x*-coordinate and the hyperbolic slope offers better approximation for vertical sections of the continental slope and shelf. The eigensolutions are available to study in detail the structures of velocity field in a linear framework as the internal waves propagate to hyperbolic topography. Noting that the solutions can only be applied to a subcritical topography. In other words, the topographic slope must be smaller than the slope of internal wave rays.

3 PROPAGATION OF INTERNAL WAVES FROM DEEP OCEAN TO HYPERBOLIC SLOPE

Considering a periodic internal wave propagating from a "deep" region of a flat bottom onto a hyperbolic slope as shown in Fig.1, a hyperbolic slope $\left(h(x)=r/x\ \ (r<0)\right)$ is connected to flat bottom of abyssal ocean whose non-dimensional depth is 1.0. $x=x_0$ is the vertical section connecting deep ocean region with hyperbolic slope region. x_0 is chosen so that the maximum slope of hyperbolic topography, i.e., $-r/x_0^2$, must be smaller than the slope of internal wave rays because only the subcritical topography is considered in this study. Generally speaking, the velocity field and the shear will change as the internal waves propagate up to a sloping topography (Müller and Liu, 2000a, b). To obtain fine structures of velocity field in hyperbolic slope region, employing the eigensolutions in Eq.14 or 15 is the key to describe evolution of internal waves and corresponding velocity field in hyperbolic regions when a periodic internal wave propagates from deep ocean.

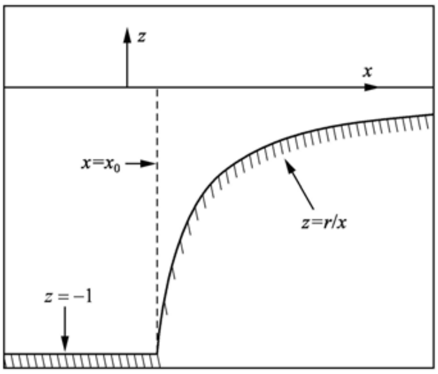

Fig.1 Schematic map of topography

Supposedly, an incoming monochromatic internal wave from deep ocean is

$$\varphi_1 = \mathrm{Re}\left\{A\sin kz \exp\left[\mathrm{i}(ckx-\omega t)\right]\right\} \tag{16}$$

where $k = n\pi$, n is the mode number of incoming wave. In general, the frequency does not change as the wave propagates to the hyperbolic slope (Müller and Liu, 2000a). Thereby, the spatial evolution of the internal waves is focused. Let:

$$\phi_1 = A\sin(kz)\exp(\mathrm{i}ckx) \tag{17}$$

Note that Eq.17 can describe only the internal wave at deep ocean region where the bottom boundary is flat. When the internal wave propagates up to a hyperbolic slope, the stream function should be described with solutions in Eqs.14, i.e.,

$$\phi_2 = \sum_{n=1}^{\infty}\sin(q_n\xi)\left[D_{1n}\exp(\mathrm{i}q_n\eta) + D_{2n}\exp(-\mathrm{i}q_n\eta)\right] \tag{18}$$

where $q_n = n\pi/\xi_0$, D_{1n}, D_{2n} the undetermined coefficients, which can be determined by the matching conditions between Eqs.18 and 17. Here, the matching conditions provided by Wunsch (1968) are used, which requires that the stream function and its gradient remain constant along the section, i.e., $\eta = \eta_0$, where

$$\eta_0 = [cx_0 - h(x_0)]^2 + [cx_0 + h(x_0)]^2.$$

ϕ_1 is only a function of ξ along the $\eta = \eta_0$ section. Extend ϕ_1 and $\partial\phi_1/\partial\eta$ into the Fourier series, we obtain:

$$\begin{aligned}\phi_1|_{\eta=\eta_0} &= \sum_{n=1}^{\infty}H_n\sin(q_n\xi) = \sum_{n=1}^{\infty}\sin(q_n\xi)\left[D_{1n}\exp(\mathrm{i}q_n\eta_0) + D_{2n}\exp(-\mathrm{i}q_n\eta_0)\right]\\ \frac{\partial\phi_1}{\partial\eta}|_{\eta=\eta_0} &= \sum_{n=1}^{\infty}I_n\sin(q_n\xi) = \sum_{n=1}^{\infty}\mathrm{i}q_n\sin(q_n\xi)\left[D_{1n}\exp(\mathrm{i}q_n\eta_0) - D_{2n}\exp(-\mathrm{i}q_n\eta_0)\right]\end{aligned} \tag{19}$$

From the above equations, one can get:

$$D_{1n} = \frac{1}{2}\left(H_n + \frac{I_n}{\mathrm{i}q_n}\right)\exp(-\mathrm{i}q_n\eta_0); D_{2n} = \frac{1}{2}\left(H_n - \frac{I_n}{\mathrm{i}q_n}\right)\exp(\mathrm{i}q_n\eta_0) \tag{20}$$

Substituting (20) into (18) yields:

$$\begin{aligned}\phi_2 &= \sum_{n=1}^{\infty}\sin(q_n\xi)\left\{\frac{1}{2}\left(H_n + \frac{I_n}{\mathrm{i}q_n}\right)\exp[\mathrm{i}q_n(\eta-\eta_0)] + \frac{1}{2}\left(H_n - \frac{I_n}{\mathrm{i}q_n}\right)\exp[\mathrm{i}q_n(\eta_0-\eta)]\right\}\\ &= \sum_{n=1}^{\infty}\sin(q_n\xi)\left\{H_n\cos[q_n(\eta-\eta_0)] + \frac{I_n}{q_n}\sin[q_n(\eta-\eta_0)]\right\}\end{aligned} \tag{21}$$

This is the expression for the evolution of incoming internal waves shown in Eq.17 at a hyperbolic slope region. In Cartesian coordinates, the solutions can be rewritten as:

$$\begin{aligned}\phi_2 = &\sum_{n=1}^{\infty}\frac{H_n}{2}\left\{\sin\left[2q_n(cx-z)^2-q_n\eta_0\right]-\sin\left[2q_n(cx+z)^2-q_n\eta_0\right]\right\}\\ &-\sum_{n=1}^{\infty}\frac{I_n}{2q_n}\left\{\cos\left[2q_n(cx-z)^2-q_n\eta_0\right]-\cos\left[2q_n(cx+z)^2-q_n\eta_0\right]\right\}\end{aligned} \tag{22}$$

The horizontal velocity corresponding to Eq.22 is:

$$\begin{aligned}u_2 = -\frac{\partial\phi_2}{\partial z} = &\sum_{n=1}^{\infty}2H_nq_n\left\{(cx-z)\cos\left[2q_n(cx-z)^2-q_n\eta_0\right]+(cx+z)\cos\left[2q_n(cx+z)^2-q_n\eta_0\right]\right\}\\ &+\sum_{n=1}^{\infty}2I_n\left\{(cx-z)\sin\left[2q_n(cx-z)^2-q_n\eta_0\right]+(cx+z)\sin\left[2q_n(cx+z)^2-q_n\eta_0\right]\right\}\end{aligned} \tag{23}$$

The vertical shear of the horizontal velocity is:

$$\begin{aligned}\frac{\partial u_2}{\partial z} = &\sum_{n=1}^{\infty}2H_nq_n\left\{-\cos\left[2q_n(cx-z)^2-q_n\eta_0\right]+\cos\left[2q_n(cx+z)^2-q_n\eta_0\right]\right\}\\ &+\sum_{n=1}^{\infty}8H_nq_n^2\left\{(cx-z)^2\sin\left[2q_n(cx-z)^2-q_n\eta_0\right]-(cx+z)^2\sin\left[2q_n(cx+z)^2-q_n\eta_0\right]\right\}\\ &+\sum_{n=1}^{\infty}2I_n\left\{-\sin\left[2q_n(cx-z)^2-q_n\eta_0\right]+\sin\left[2q_n(cx+z)^2-q_n\eta_0\right]\right\}\\ &+\sum_{n=1}^{\infty}8I_nq_n\left\{-(cx-z)^2\cos\left[2q_n(cx-z)^2-q_n\eta_0\right]+(cx+z)^2\cos\left[2q_n(cx+z)^2-q_n\eta_0\right]\right\}\end{aligned} \tag{24}$$

The horizontal velocity and the vertical shear of the incoming wave ϕ_1 at deep ocean are:

$$u_1 = -\frac{\partial\phi_1}{\partial z} = -Ak\cos(kz)\exp(\mathrm{i}ckx) \tag{25}$$

$$\frac{\partial u_1}{\partial z} = Ak^2\sin(kz)\exp(\mathrm{i}ckx) \tag{26}$$

The real parts of ϕ_1, u_1, $\partial u_1/\partial z$ multiplied by $\exp(-\mathrm{i}\omega t)$ are, respectively, the stream function, horizontal velocity, and shear of the incoming wave at deep ocean region while the real parts of ϕ_2, u_2, $\partial u_2/\partial z$ multiplied by $\exp(-\mathrm{i}\omega t)$ are those of the evolution of incoming internal wave propagating up to a hyperbolic slope region.

Fig.2 gives an example of the stream function of internal waves propagating from deep ocean to hyperbolic slope. In this figure, the hyperbolic slope begins with $x_0 = 10.1$ and ends at x=70. r= –10.1 is chosen so that the maximum topographic slope is 0.099. The slope of incoming wave rays is 0.1 and the mode number is one, i.e., $k=\pi$. It is evident that the wavelength becomes smaller as internal wave propagates from deep ocean to hyperbolic slope. The pattern of stream function also changes at the same period. In the deep ocean region, the streamlines are like a regular ellipse, while over the hyperbolic slope, the ellipse becomes irregular. The vertical section $x = 10.1$ is the section that connects the hyperbolic slope region with the deep ocean region. The stream function is smooth near this section, which implies that the matching conditions provided by Wunsch (1968) work well.

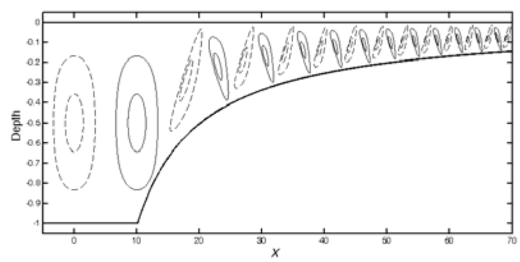

Fig.2 Streamlines of internal wave propagating from deep ocean to hyperbolic slope. The slope of incoming wave rays is 0.1 and the mode number is one

The solid line denotes the positive values of stream function and the dashed line, the negative values

Fig.3 shows the stream function, the horizontal velocity, and the vertical shear of horizontal velocity along the horizontal transect z=-0.05, while the

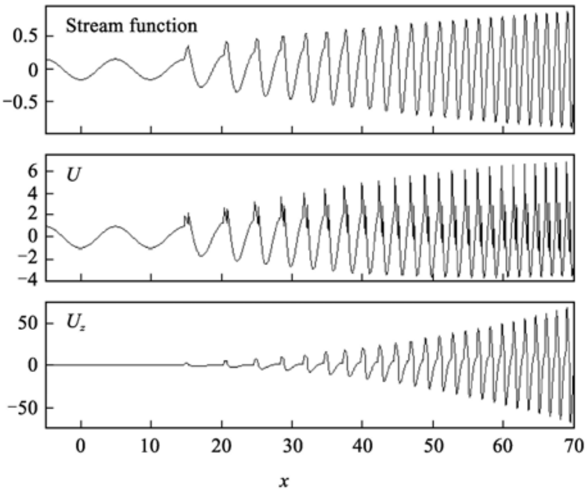

Fig.3 The normalized stream function, horizontal velocity (*U*), and the vertical shear of horizontal velocity (U_Z) along *z*=-0.05. The slope of incoming wave rays is 0.2 and the mode number is one

The parameters of topography are the same as those in Fig.2

topography is the same as that in Fig.2. The slope of incoming wave rays is 0.2 and the mode number is one. The stream function, velocity, and velocity shear have been normalized respectively by the maximum values in the deep ocean region, which means that one is the maximum values of the absolute stream function, velocity, and velocity shear in a deep ocean region. Then, the enhancement of velocity and velocity shear can be obviously observed when internal waves propagates up to a hyperbolic slope. Note that $x = 10.1$ is the case of section that connects deep ocean region with the hyperbolic slope. It is obvious that the amplitude of normalized horizontal velocity over the slope region is larger than one, and the amplitude becomes larger when water depth is shallower. The normalized velocity shear shows similar behavior to the velocity. The maximum value of the normalized velocity in hyperbolic slope region is larger than 6.0, while the maximum value of the normalized shear is even larger than 50. It means that the velocity and velocity shear increase evidently as the internal waves propagate to a hyperbolic slope, which is consistent with previous studies (Wunsch 1968; Müller and Liu, 2000a, b).

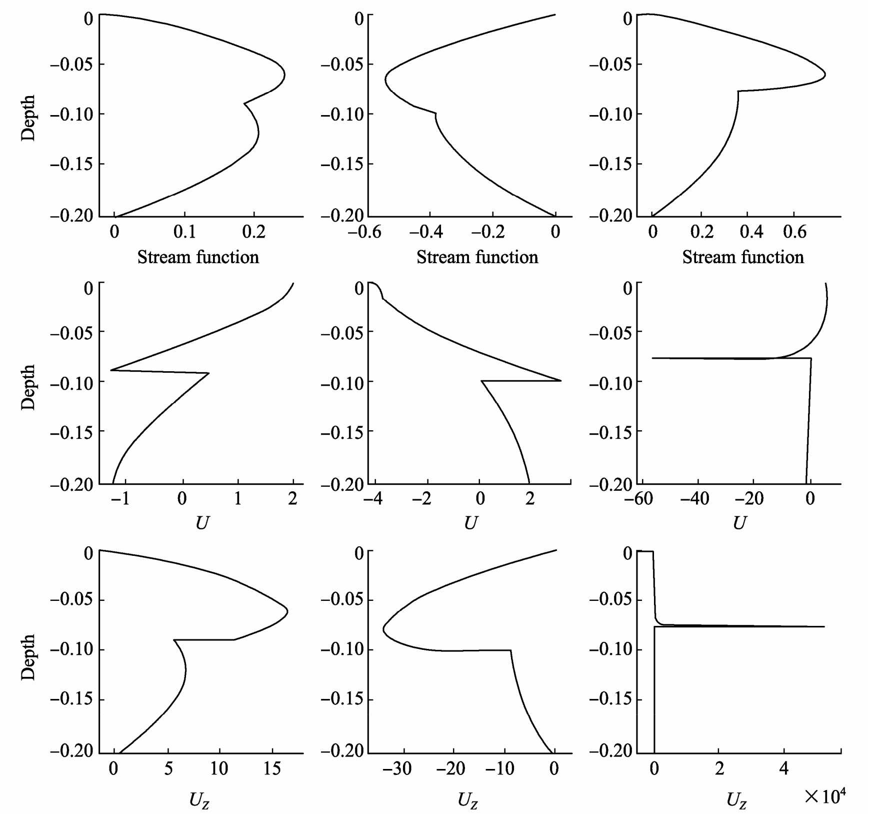

Fig.4 The normalized stream function, horizontal velocity (*U*), and the vertical shear of horizontal velocity (U_Z) along *x*=50 when *c*=0.3 (left panel), ***c*=0.2** (middle panel)**, and *c*=0.1** (right panel)**. The mode number of incoming waves is one**

The parameters of topography are the same as those in Fig.2

For a selected hyperbolic topography, the slope of internal wave rays (*c*) also has influence on the distribution of the velocity and velocity shear. Fig.4 shows the stream function, horizontal velocity, and the vertical shear of horizontal velocity along vertical section $x = 50$ when *c*=0.3 (left panel), *c*=0.2 (middle panel), and *c*=0.1 (right panel). The topography is the same as that in Fig.2. The variables have been normalized with the respective maximum values of deep ocean region. Fig.4 shows that the maximum values of absolute velocity and velocity shear when *c*=0.2 are lager than those when *c*=0.3, and when *c*=0.1 the values are larger than those when *c*=0.2. The velocity and velocity shear show extreme large values in the right panel where the slope of internal wave rays is 0.1 which is close to the maximum topographic slope 0.099. It agrees with previous theoretical studies showing the wave reflected from the topography has infinite velocity and velocity shear when the slope of internal wave rays is equal to the topographic slope. Similar behaviors can be found along other vertical sections of hyperbolic slope region.

When the velocity shear is large enough, the Richardson numbers may significantly decrease so that instability occurs, leading to overturning and mixing (Phillips, 1977). Moreover, internal waves will evolve into internal solitons when internal waves propagate to a continental slope (Liu et al., 1998; Cai et al., 2001; Fang and Du, 2005). However, the instability and the nonlinear evolution process should not be the case of this study that deals with linear theory only. Even though, the eigensolutions of internal waves at continental slope and shelf may help estimating the diapycnal mixing induced by internal waves. Further study is demanded on the nonlinear process.

4 SUMMARY

This study concerns the linear evolution of internal waves propagating from deep ocean to continental slope and shelf. The hyperbolic slope rather than the linear slope is used to describe the continental slope and shelf. A transformation, which can convert the hyperbolic slope in a physical space to a flat bottom in transformation space while the governing equations of internal waves remain hyperbolic, was developed to obtain the eigensolutions of internal waves over the hyperbolic slope in a two-dimensional and linear framework. The obtained eigensolutions were then applied to the propagation of internal waves from deep ocean to hyperbolic slope. The results show that the velocity and the velocity shear increased when internal waves propagates to the hyperbolic slope. Especially, when the slope of internal wave rays approached to the topographic slope, the velocity and the velocity shear showed extreme large value, which is similar to the results of previous studies. The extreme large values of velocity and velocity shear would lead to instability and mixing. However it was the linear framework that used in this study. Therefore, the instability process cannot be described. Further study in the future is demanded to describe the internal-wave-induced diapycnal mixing.

References

Baines, P. G., 1971a. The reflexion of internal/inertial waves from bumpy surfaces. *J. Fluid. Mech.* **46**: 273-291.

Baines, P. G., 1971b. The reflexion of internal/inertial waves from bumpy surfaces, Part 2: Split reflexion and diffraction. *J. Fluid. Mech.* **49**: 113-131.

Cai, S. Q. and Z. J. Gan, 2001. Progress in the study of the internal soliton in the northern South China Sea. *Advance in Earth Sciences* **16** (2): 215-219.

Dai D. J., W. Wang, F. L. Qiao and Y. L. Yuan, 2005. Scattering process of internal waves propagating over a subcritical strait slope onto a shelf region. *Journal of Ocean university of China* **4**(4): 377-382.

Fang, X. H. and T. Du, 2005. Fundamentals of Oceanic Internal Waves and Internal Waves in the China Seas. China Ocean University Press, Qingdao. p. 337.

Lamb, K. G., 1994. Numerical experiments of internal wave generation by strong tidal flow across a finite amplitude bank edge. *J. Geophys. Res.* **99**(C1): 843-864.

Liu, A. K., Y. S. Chang, M. K. Hsu and N. K. Liang, 1998. Evolution of nonlinear internal waves in the East and South China Seas. *J. Geophys. Res.* **103**: 7 995-8 008.

Müller, P. and X. Liu, 2000a. Scattering of internal waves at finite topography in two dimensions, I theory and case studies. *J. Phys. Oceanogr*. **30**: 532-549.

Müller, P. and X. Liu, 2000b. Scattering of internal waves at finite topography in two dimensions, II spectral calculations and boundary mixing. *J. Phys. Oceanogr*. **30**: 550-563.

Nash J. D., E. Kunze, C. M. Lee and T. B. Sanford, 2006. Structure of the baroclinic tide generated at Kaena ridge, Hawaii. *J. Phys. Oceanogr.* **36**: 1 123-1 135.

Petrelis F., S. Llewellyn Smith and W. R. Young, 2006. Tidal conversion at a submarine ridge. *J. Phys. Oceanogr.* **36**: 1 053-1 071.

Phillips, O. M., 1977. The Dynamics of the Upper Ocean, Cambridge University Press, London. p. 336.

Vlasenko,V., N. Stashchuk, K. Hutter, 2005. Baroclinic Tide: Theoretical Modeling and Observational Evidence. Cambridge University Press, London. p. 351.

Wunsch, C., 1968. On the propagation of internal waves up a slope. *Deep-Sea Research* **15**: 251-258.

Wunsch C. and R. Ferrari, 2004. Vertical mixing, energy, and the general circulation of the oceans. *Annual Review of Fluid Dynamics* **36**: 281-314.

Appendix A: internal wave equations

For a continental slope, a dextral Cartesian coordinate system is set up as follows; $\tilde{x}$ represents a cross-slope axis positive shoreward, $\tilde{y}$ represents an axis along the continental slope, and $\tilde{z}$, a vertical axis positive up. In most of real ocean, the length of continental slope, i.e., the scale along the continental slope, is generally much larger than the width. It implies that the gradients of variables along $\tilde{y}$ axis can be ignored compared with those along $\tilde{x}$ axis. However, the velocity component along $\tilde{y}$ axis must be included because the Coriolis Effect is important for some linear internal waves. Then in two-dimensional framework, the linear internal waves obey (Lamb, 1994; Vlasenko et al., 2005):

$$\frac{\partial \tilde{u}}{\partial \tilde{t}} - \tilde{f}\tilde{v} = -\frac{1}{\bar{\tilde{\rho}}_0}\frac{\partial \tilde{p}}{\partial \tilde{x}} \tag{A1}$$

$$\frac{\partial \tilde{v}}{\partial \tilde{t}} + \tilde{f}\tilde{u} = 0 \tag{A2}$$

$$\frac{\partial \tilde{w}}{\partial \tilde{t}} = -\frac{1}{\bar{\tilde{\rho}}_0}\frac{\partial \tilde{p}}{\partial \tilde{z}} - \frac{\tilde{\rho}'}{\bar{\tilde{\rho}}_0}\tilde{g} \tag{A3}$$

$$\frac{\partial \tilde{u}}{\partial \tilde{x}} + \frac{\partial \tilde{w}}{\partial \tilde{z}} = 0 \tag{A4}$$

$$\frac{\partial \tilde{\rho}'}{\partial \tilde{t}} + \tilde{w}\frac{\partial \tilde{\rho}_0}{\partial \tilde{z}} = 0 \tag{A3}$$

where $(\tilde{u},\tilde{v},\tilde{w})$ are the three velocity components corresponding to $(\tilde{x},\tilde{y},\tilde{z})$, $\tilde{p}$ the pressure, $\tilde{f}$ the Coriolis parameter, $\tilde{\rho}_0 = \tilde{\rho}_0(z)$ the density in static equilibrium, $\tilde{\rho}'$ the density perturbation from this state due to the wave motion, $\bar{\tilde{\rho}}_0$ the mean value of $\tilde{\rho}_0$, $\tilde{g}$ the acceleration due to gravity.

From Eqs. (A1) and (A2), one can obtain

$$\frac{\partial^2 \tilde{u}}{\partial \tilde{t}^2} + \tilde{f}^2\tilde{u} = -\frac{1}{\bar{\tilde{\rho}}_0}\frac{\partial^2 \tilde{p}}{\partial \tilde{x}\partial \tilde{t}} \tag{A6}$$

$\dfrac{\partial (A3)}{\partial t} - \tilde{f}\times(A2)$ yields

$$\frac{\partial^2 \tilde{w}}{\partial \tilde{t}^2} + \tilde{N}^2\tilde{w} = -\frac{1}{\bar{\tilde{\rho}}_0}\frac{\partial^2 \tilde{p}}{\partial \tilde{z}\partial \tilde{t}} \tag{A7}$$

where $\tilde{N} = (-\dfrac{\tilde{g}}{\bar{\tilde{\rho}}_0}\dfrac{\partial \tilde{\rho}_0}{\partial \tilde{z}})^{\frac{1}{2}}$, the Brunt-Väisälä frequency, which will be assumed to be a constant in this study.

$\dfrac{\partial (A7)}{\partial x} - \dfrac{\partial (A6)}{\partial z}$ yields

$$\frac{\partial^3 \tilde{w}}{\partial \tilde{x}\partial \tilde{t}^2} + \tilde{N}^2\frac{\partial \tilde{w}}{\partial \tilde{x}} - \frac{\partial^3 \tilde{u}}{\partial \tilde{z}\partial \tilde{t}^2} - \tilde{N}^2\frac{\partial \tilde{u}}{\partial \tilde{z}} = 0 \tag{A8}$$

Introduce the stream function, $\tilde{\varphi}$, which lets $\tilde{u} = -\dfrac{\partial \tilde{\varphi}}{\partial \tilde{z}}, \tilde{w} = \dfrac{\partial \tilde{\varphi}}{\partial \tilde{x}}$, the above equation can be reduced to

$$\frac{\partial^4 \tilde{\varphi}}{\partial \tilde{x}^2\partial \tilde{t}^2} + \frac{\partial^4 \tilde{\varphi}}{\partial \tilde{z}^2\partial \tilde{t}^2} + \tilde{f}^2\frac{\partial^2 \tilde{\varphi}}{\partial \tilde{z}^2} + \tilde{N}^2\frac{\partial^2 \tilde{\varphi}}{\partial \tilde{x}^2} = 0 \tag{A9}$$

For monochromatic waves of frequency $\tilde{\omega}$, defines $\tilde{\varphi} = \tilde{\phi}\exp(\mathrm{i}\tilde{\omega}\tilde{t})$, then the other wave variables are given by

$$\tilde{v} = \frac{\tilde{f}}{\mathrm{i}\tilde{\omega}}\tilde{\varphi}_{\tilde{z}} \tag{A10}$$

$$\tilde{p}_{\tilde{x}} = -\bar{\tilde{\rho}}_0 \frac{\tilde{\omega}^2 - \tilde{f}^2}{\mathrm{i}\tilde{\omega}}\tilde{\varphi}_{\tilde{z}} \tag{A11}$$

$$\tilde{\rho}' = \frac{\bar{\tilde{\rho}}_0}{\tilde{g}}\frac{\tilde{N}^2}{\mathrm{i}\tilde{\omega}}\tilde{\varphi}_{\tilde{x}} \tag{A12}$$

Appendix B: derivation of internal wave equation in transformation space

For an internal wave equation

$$\phi_{zz} - \frac{1}{c^2}\phi_{xx} = 0 \tag{B1}$$

assume the following transformation:

$$\begin{cases} \xi = (cx - z)^2 - (cx + z)^2 \\ \eta = (cx - z)^2 + (cx + z)^2 \end{cases} \tag{B2}$$

We have

$$\begin{aligned} &\frac{\partial \xi}{\partial z} = -2(cx - z) - 2(cx + z), \quad \frac{\partial \xi}{\partial x} = 2c(cx - z) - 2c(cx + z), \\ &\frac{\partial \eta}{\partial z} = -2(cx - z) + 2(cx + z), \quad \frac{\partial \eta}{\partial x} = 2c(cx - z) + 2c(cx + z), \\ &\frac{\partial^2 \xi}{\partial z^2} = 0, \quad \frac{\partial^2 \xi}{\partial x^2} = 0, \quad \frac{\partial^2 \eta}{\partial z^2} = 0, \quad \frac{\partial^2 \eta}{\partial x^2} = 0 \end{aligned} \tag{B3}$$

Due to

$$\frac{\partial \phi}{\partial z} = \frac{\partial \phi}{\partial \xi}\frac{\partial \xi}{\partial z} + \frac{\partial \phi}{\partial \eta}\frac{\partial \eta}{\partial z}$$

$$\frac{\partial \phi}{\partial x} = \frac{\partial \phi}{\partial \xi}\frac{\partial \xi}{\partial x} + \frac{\partial \phi}{\partial \eta}\frac{\partial \eta}{\partial x}$$

$$\frac{\partial^2 \phi}{\partial z^2} = \frac{\partial^2 \phi}{\partial \xi^2}(\frac{\partial \xi}{\partial z})^2 + \frac{\partial^2 \phi}{\partial \eta^2}(\frac{\partial \eta}{\partial z})^2 + 2\frac{\partial^2 \phi}{\partial \xi \partial \eta}\frac{\partial \xi}{\partial z}\frac{\partial \eta}{\partial z} + \frac{\partial \phi}{\partial \xi}\frac{\partial^2 \xi}{\partial z^2} + \frac{\partial \phi}{\partial \eta}\frac{\partial^2 \eta}{\partial z^2} \tag{B4}$$

$$\frac{\partial^2 \phi}{\partial x^2} = \frac{\partial^2 \phi}{\partial \xi^2}(\frac{\partial \xi}{\partial x})^2 + \frac{\partial^2 \phi}{\partial \eta^2}(\frac{\partial \eta}{\partial x})^2 + 2\frac{\partial^2 \phi}{\partial \xi \partial \eta}\frac{\partial \xi}{\partial x}\frac{\partial \eta}{\partial x} + \frac{\partial \phi}{\partial \xi}\frac{\partial^2 \xi}{\partial x^2} + \frac{\partial \phi}{\partial \eta}\frac{\partial^2 \eta}{\partial x^2}$$

Eq.B1 is transformed to

$$\frac{\partial^2 \phi}{\partial \xi^2}[16(cx - z)(cx + z)] + \frac{\partial^2 \phi}{\partial \eta^2}[-16(cx - z)(cx + z)] = 0 \tag{B5}$$